Equivalent Circuit of Mush Wound AC Windings for High Frequency Analysis

Gabriele Grandi, Domenico Casadei, Ugo Reggiani
Department of ELECTRICAL ENGINEERING
Viale Risorgimento 2 , I-40136, Bologna - Italy
Ph. +39 51 644 3571, fax +39 51 644 3588
E-mail: elettrot5@dns.ing.unibo.it

Abstract - **The paper describes a lumped parameter equivalent circuit for the HF analysis of mush wound coils of AC windings. The equivalent circuit takes account of turn-to-turn and turn-to-iron stray capacitances. Dissipative phenomena due to eddy currents in the coil wires and the laminated iron core are also considered. The parameter identification is based on sinusoidal impedance measurements on a test coil. The model of a multi-coil AC stator winding can be easily derived from the proposed equivalent circuit. This model allows one to predict both common- and differential-mode conducted EMI in switching converters supplying AC motors. The simulation results obtained by PSpice are in good agreement with the experimental data.**

I. INTRODUCTION

A HF model for AC windings is required to predict the voltage distribution across the coils, common- and differential-mode currents in inverter-fed motor drives and, in general, conducted interferences up to some tens of megahertz in AC power mains.

Detailed winding models for large AC motors have been previously developed. Most of these studies concern AC motors having the windings in "form wound coils" with a given structure [1]-[4]. Little was published concerning the modeling of AC motors with the windings in "mush wound coils" [5]-[7]. In this type of winding the high number of turns and their random assembling make the determination of an equivalent circuit a hard task.

Under the influence of a high frequency excitation, the behavior of the stator iron core is completely different from that shown in the case of a power frequency excitation. At high frequencies, eddy currents cause the iron enclosing a stator coil to act as a barrier for the magnetic flux. As a consequence, the self and mutual inductances of the coils change with frequency. Owing to skin and proximity effects, the coil resistance also changes. Furthermore, the coil model must take turn-to-turn and turn-to-iron capacitances into account. The turn-to-iron capacitances lead to a three-terminal equivalent circuit, being the motor frame usually grounded.

The random nature of a mush wound coil, with turns at unknown locations inside the slots, makes modeling based on the series connection of single turn equivalent circuits as more difficult as the number of turns increases. In this paper, a lumped parameter circuit which has a sinusoidal impedance equal to that of the test coil in a given frequency range is proposed. In order to highlight the influence of the laminated iron core, mush wound coils with an air core are considered as a preliminary approach. Then, real coils with a laminated iron core are analyzed and an extrapolation procedure to determine the coil inductance variation with frequency is presented.

II. WINDING INDUCTANCE

A mush wound coil for AC stator windings is considered. The coil consists of N turns connected in series and having a circular cross-section. A schematic drawn of the coil geometry is given in Fig. 1.

The distribution of the N turns in the coil cross-section is random in both the slot region and the overhang region. Fig. 2 shows the cross-sectional view of the turns inside the slot.

Under the assumption of an uniform current density distribution, the inductance of a coil with N turns can be calculated multiplying by N^2 the inductance of a single turn having the same cross-section of the coil

$$L_{(\text{turns} = N,\ \text{diam.} = d_w)} = N^2 \cdot L_{(\text{turns} = 1,\ \text{diam.} = D_c)} . \qquad (1)$$

The assumption that the current density is uniformly distributed over the coil cross-section (diameter D_c in Fig. 2) is satisfied in spite of skin and proximity effects, if the turn number N is high enough (i.e., tens of turns at least). As it is shown in Fig. 1, each turn of the coil consists of two semi-circular or rectangular wires in the overhang region and two parallel straight wires in the slot region.

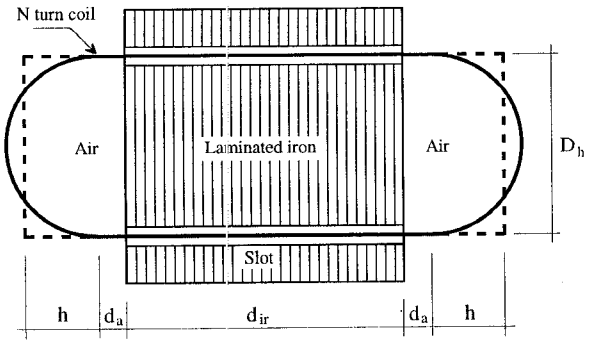

Fig. 1. Schematic drawn of the coil geometry

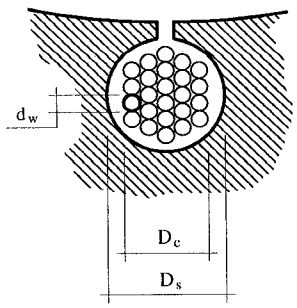

Fig. 2. Cross-sectional view of the turns inside the slot

For the coil inductance calculation, the semi-circular overhangs are replaced by rectangular overhangs having the same area. With reference to Fig. 1, we obtain

$$h = \frac{\pi D_h}{8} . \qquad (2)$$

A. Air-core Coil

As a first step of the analysis, we consider a coil with the same geometry of the real coil but placed in a linear and homogeneous medium (air).

The coil inductance L^* is calculated considering the contribution of both the external and internal inductances

$$L^* = L^*_{ext} + L^*_{int} . \qquad (3)$$

We can calculate the external inductance by the concept of "partial inductance" described in [8]. In this case, the radius of the wire is $r_c = D_c/2$ and the rectangular loop has side lengths $a = 2h+2d_a+d_{ir}$ and $b = D_h$, as represented in Fig. 1. From the formula derived in [8] and from (1), we can write

$$L^*_{ext} = \left[2\left(L^*_{pa} - M^*_{pa}\right) + 2\left(L^*_{pb} - M^*_{pb}\right)\right] N^2 . \qquad (4)$$

The expressions of self and mutual partial inductances are given in the Appendix.

The contribution of the internal inductance is usually negligible. However, under the assumption of an uniform current density distribution in the coil cross-section, L^*_{int} can be calculated with a good approximation through the DC internal inductance per-unit-length of a straight round wire. As it is known, this inductance is $\mu_o/8\pi$ for any wire radius. Then, taking (1) into account, we obtain

$$L^*_{int} = \frac{\mu_o}{4\pi} (a+b) N^2 . \qquad (5)$$

B. Real Coil

In this case, we assume that the coil inductance L is given by the sum of the inductance L^{air} of the wires in the overhang region and the inductance L^{iron} of the wires in the slot region

$$L = L^{air} + L^{iron} . \qquad (6)$$

This assumption is satisfied with a good accuracy. In fact, the flux lines produced by the currents in the overhangs mainly lie in planes perpendicular to the iron laminations. These flux lines do not penetrate the iron core owing to the shielding effect of eddy currents which can freely circulate in the iron sheets.

On the basis of the previous considerations, we can calculate the inductance L^{air} related to the overhangs by the image method [9]. This approach leads to consider the inductance of a rectangular air-core loop having side lengths $a = 2h+2d_a$ and $b = D_h$ with a wire radius $r_c = D_c/2$. Also in this case, we can apply the method of partial inductances and (4) can be employed to calculate the external inductance L^{air}_{ext}. The internal inductance L^{air}_{int} can be obtained by (5). Thus, the overhang inductance L^{air} is given by

$$L^{air} = L^{air}_{ext} + L^{air}_{int} . \qquad (7)$$

With reference to the inductance L^{iron}, we can note that this contribution is strongly affected by the frequency. In fact, the core lamination opposes eddy currents so that the shielding effect becomes significant only at high frequencies. As a consequence, the skin depth of the magnetic field produced by the currents in the slots decreases as the frequency increases. This has been confirmed in previous works [3], [4] and by the experimental tests described below. In particular, it has been verified that only for frequencies above several megahertz the magnetic field does not penetrate the laminated iron core. For this reason, the determination of the coil inductance requires an accurate and difficult field analysis taking eddy currents and core lamination into account. However, neglecting the magnetic field penetration inside the laminated iron core, the inductance L^{iron} can be evaluated as the inductance of a group of N parallel straight wires surrounded by an ideal magnetic cylindrical shield. The following expression is obtained

$$L^{iron} = \frac{\mu_o}{\pi}\left(\frac{1}{4} + \ln\frac{D_s}{D_c}\right) d_{ir} N^2 , \qquad (8)$$

where $2d_{ir}$ is the wire length and D_s the shield internal diameter. The value calculated by (8) can be considered as the asymptotic lower limit of the slot contribution to the overall inductance of the coil.

C. Experimental Tests

In order to verify the previous considerations, both air- and laminated iron-core coils were built, with a number of turns N = 63. The corresponding dimensions are given in Table I of the Appendix.

Fig. 3 shows the measured values of the inductance of the two coil types as a function of frequency (solid lines with black dots).

The calculated value for the air-core coil inductance is $L^* = 1030$ μH. As Fig. 3 shows, the measured values of L^* are in good agreement with the calculated value. Skin and proximity effects in the copper wires are responsible for the slight decrease in the measured inductance in the low-frequency range. The turn-to-turn parasitic capacitances cause the sudden increase in the inductance above 80 kHz. The last measurable point is at about 200 kHz owing to the capacitive behavior of the coil for higher frequencies.

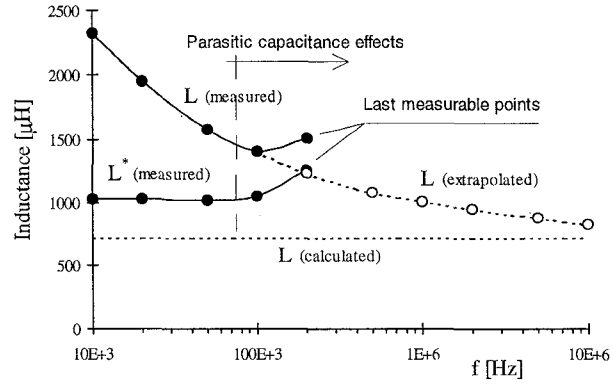

Fig. 3. Coil inductance for N=63

With reference to the laminated iron-core coil, Fig. 3 shows a continuous decrease in the inductance L. As discussed above, this decrease is due to the shielding effect of the eddy-currents than can flow in the iron core in spite of its lamination. Also in this case, the inductance measurements can be performed only up to 80 kHz owing to turn-to-turn and turn-to-iron parasitic capacitances. The effects of these parasitic parameters will be discussed in Sections III and IV.

D. Extrapolation of the Real Coil Inductance

In order to extend the inductance measurements to the high-frequency range, coils with a reduced number of turns were built. In this way, the parasitic capacitive effects are reduced and the parallel resonances are shifted at higher frequencies. It has been found that the ratio r^* between the inductance L of a real coil and the inductance L^* of the corresponding air-core coil practically does not depend on the number of turns in a wide frequency range.

Fig. 4 shows the ratio r^* as a function of frequency for N = 1, 2, 3, 4, and 63. This figure confirms that the inductance ratio does not depend on the number of turns for excitation frequencies above 50 kHz. As a consequence, we can characterize the magnetic behavior of a laminated iron-core coil in a wide frequency range by measuring the inductance of a coil with a low number of turns so avoiding the effects of parasitic capacitances. Then, the extrapolation of the inductance of a real coil with any turn number can be performed measuring or calculating by (3) the corresponding air-core coil inductance and multiplying by the value of r^* at the desired frequency

$$L(f) = L^* r^*(f) . \qquad (9)$$

The results of the inductance extrapolation up to 10 MHz for a laminated iron-core coil with N = 63 turns are represented in Fig. 3. It can be noted the good agreement between the extrapolated asymptote and the inductance value L = 720 μH calculated by (6), (7), and (8) in the case of magnetic field confined inside the slot. It can also be observed that L assumes the value of L^* at the frequency of about 1 MHz. For higher frequencies the real coil inductance is lower than the corresponding air-core coil inductance.

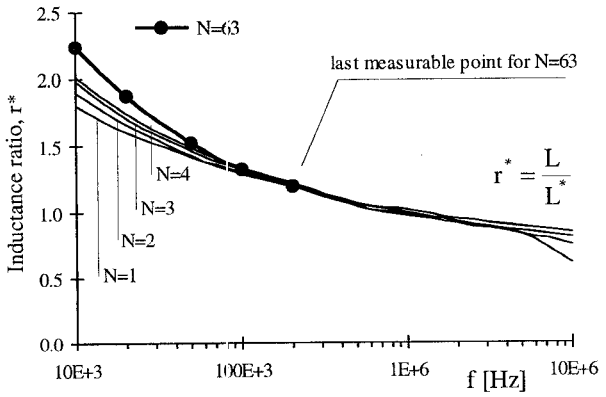

Fig. 4. Measured inductance ratio r^* vs. frequency

III. HF MODEL OF THE COIL

The HF circuit model of a mush wound coil for AC windings must take account of turn-to-turn and turn-to-iron capacitances. Furthermore, dissipative phenomena such as skin and proximity effects in the wires, dielectric and iron losses should be included.

A model could be derived assuming the coil made of turns connected in series, with each turn represented by an equivalent circuit including also mutual effects between turns. However, this approach can be used only when the turn number is sufficiently low and the coil geometry is known inside and outside the slots. This is the case of large AC machines with form wound coils [1], [2], [3], [4]. For small and medium AC machines, in which the turn number is high and the turns are randomly wound, a different approach must be employed.

The approach developed in this paper is based on the equivalence between the coil and the circuit model in terms of sinusoidal impedance $\mathbf{Z}_c$. Hence, both the real part (equivalent series resistance, R_S) and the imaginary part (equivalent series reactance, X_S) of the impedance $\mathbf{Z}_c$ are considered (Fig. 5).

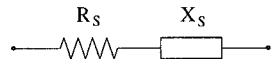

$$\mathbf{Z}_c = R_s + jX_s$$

Fig. 5. Series representation of the sinusoidal impedance

In order to emphasize the contribution and the effect of the laminated iron core at high frequencies, firstly the analysis is developed for an air-core coil having the same geometry of the real coil, as in Section II.

A. Air-core Coil

To determine a suitable HF equivalent circuit of a mush wound coil with an air-core, it is necessary to perform measurements of its sinusoidal impedance at different frequencies and to make an accurate analysis of the results. The measurements have been performed by using a programmable RLC meter HP 4192 with the frequency ranging from a few tens of kilohertz to a few megahertz. In this range, only one parallel resonance associated with dissipative phenomena has been observed. Then, an equivalent circuit whose response simulates this behavior is shown in Fig. 6.

The parameter R^*_L represents the AC wire resistance. The value of this resistance is a function of the excitation frequency owing to skin and proximity effects. If the analysis is performed in the frequency domain, the resistance variation could be modeled by a square-root function of frequency [5]. However, this variable parameter cannot be introduced in the equivalent circuit when the coil model has to be used for the transient analysis in the time domain. In this case, the resistance variation can be modeled by a proper sub-circuit. There are two kinds of circuits that can be fitted for the time domain representation of eddy currents in windings: Foster circuits (parallel or series) and Cauer circuits (standard or dual) [10]. Anyway, skin and proximity phenomena affect the air-core coil behavior only up to few hundred kilohertz which is the lower bound of the considered frequency range. For this reason, the value of the coil resistance is fixed at a mean value. In this way a simple equivalent circuit can be adopted for both the frequency and time domain analysis.

The resistors R^*_C and R^*_p must take account of the dissipative phenomena due to HF capacitive currents and dielectric losses. The series resistances R^*_L and R^*_C are in the order of the tens of ohm and the parallel resistance R^*_p of the hundreds of kilohm. In order to fit the model with the experimental results, an identification problem must be solved. An initial estimate of the air-core coil inductance L^* is obtained from (3). Owing to the random distribution of the turns, the overall parasitic capacitance C^* cannot by calculated on the basis of the coil geometry as in [11]. The overall parasitic capacitance can be determined by

$$C^* = \frac{1}{4\pi^2 f_o^2} \frac{1}{L^*}, \qquad (10)$$

where f_o is the resonant frequency.

The identification problem can be solved by a simple trial and error method or some more sophisticated numerical techniques such as the least squares method.

The measured and calculated values of the series equivalent resistance R_s and reactance X_s as a function of frequency are represented in Fig. 7. The corresponding values of the model parameters are given in Table II of the Appendix. In Fig. 7 the frequency ranges from 300 to 600 kHz in order to clearly show the matching between measured and calculated results in the resonance region. However, the agreement is still good in a wider frequency range, as it is shown in Fig. 8 where the impedance magnitude is represented in a bi-logarithmic scale.

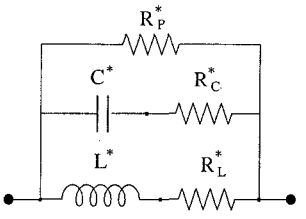

Fig. 6. HF equivalent circuit for the air-core coil

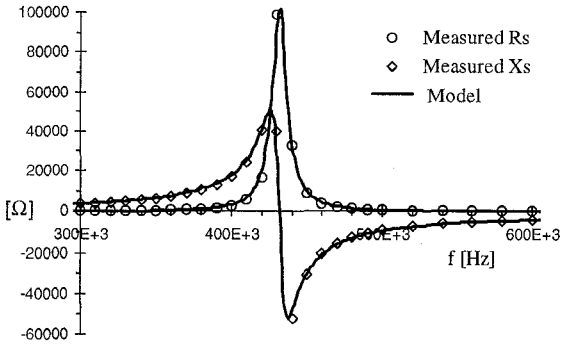

Fig. 7. Measured and calculated R_S and X_S (air-core coil)

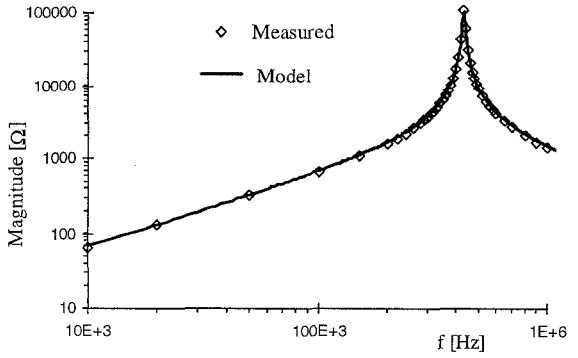

Fig. 8. Measured and calculated impedance $\mathbf{Z}_C$ (air-core coil)

B. Real Coil

Experimental tests on several iron-core coils have been carried out. In the considered frequency range a pair of parallel resonances with large dissipative phenomena has been observed in all cases. The additional dissipative phenomena are related to the AC iron losses. A suitable equivalent circuit can be represented by the series connection of two circuits having the same topology described in Section III.A. The resulting circuit model is represented in Fig. 9. Also in this case, in order to determine the model parameters on the basis of the experimental results, an identification problem must be solved.

The AC iron losses can be modeled with both an increase in the series resistances R_{L1} and R_{L2} , and a decrease in the parallel resistances R_{p1} and R_{p2} with respect to the case of the air-core coil.

The overall inductance L of the iron-core coil can be evaluated by the extrapolation method proposed in Section II.D. The results obtained for a coil with N=63 turns are represented in Fig. 3. In order to obtain an equivalent circuit valid for both the frequency and time domain analysis, the frequency dependence of L has been neglected and the constant value L = 1150 μH has been assumed in the frequency range of interest (i.e., above 100 kHz).

An alternative approach could be that of introducing a proper sub-circuit to model the resistance and inductance variations with frequency. In this case, a dual form of the

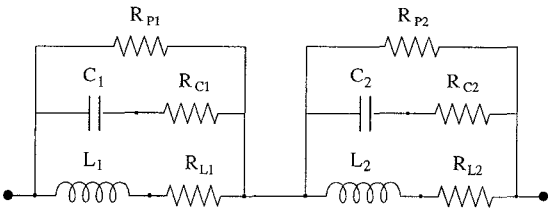

Fig. 9. HF equivalent circuit for the real coil

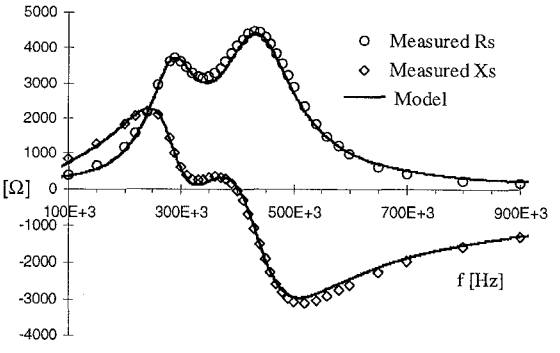

Fig. 10. Measured and calculated R_S and X_S (real coil)

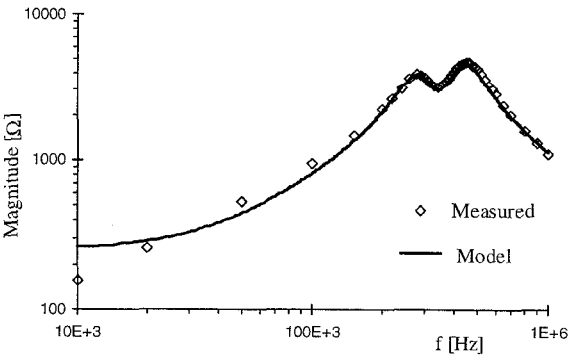

Fig. 11. Measured and calculated impedance $\mathbf{Z}_C$ (real coil)

standard Cauer can be employed as explained in [10].

An initial estimate of the reactive parameters L_1, L_2, C_1, and C_2 can be obtained solving the following equations

$$\omega_1^2 = \frac{1}{\tilde{L}_1 \tilde{C}_1}, \quad \omega_2^2 = \frac{1}{\tilde{L}_2 \tilde{C}_2},$$
$$L = \tilde{L}_1 + \tilde{L}_2, \quad \frac{1}{C} = \frac{1}{\tilde{C}_1} + \frac{1}{\tilde{C}_2}, \qquad (11)$$

where ω_1 and ω_2 are the angular frequencies corresponding to the two peaks of the measured curve $R_s(\omega)$, L is the overall inductance previously evaluated, and C the overall stray capacitance obtained by the coil reactance measured at a frequency above the resonant frequencies.

Equations (11) lead to the initial estimates

$$\tilde{L}_1 = \frac{1/C - \omega_2^2 L}{\omega_1^2 - \omega_2^2}, \quad \tilde{L}_2 = \frac{1/C - \omega_1^2 L}{\omega_2^2 - \omega_1^2},$$
$$\tilde{C}_1 = \frac{1-(\omega_2/\omega_1)^2}{1/C - \omega_2^2 L}, \quad \tilde{C}_2 = \frac{1-(\omega_1/\omega_2)^2}{1/C - \omega_1^2 L}. \qquad (12)$$

The measured and calculated values of the series equivalent resistance R_s and reactance X_s are shown in Fig. 10. The parameter values of the circuit model are given in Table III of the Appendix. Fig. 10 shows a good agreement between the calculated and measured results. In Fig. 11 the impedance magnitude is plotted in the frequency range of 0.01-1 MHz. The agreement is still good. Only in the low-frequency range we observe a discrepancy. As widely discussed above, this is due to the fact that the coil resistance and inductance change with the excitation frequency, whereas in the equivalent circuit the corresponding parameters are kept constant.

IV. MODELING THE COIL-TO-IRON CAPACITIVE COUPLING

The laminated iron core is electrically connected to the motor frame. Since the motor frame is usually grounded for safety reasons, a three-terminals equivalent circuit of the coil including turn-to-ground capacitances should be considered for HF analysis. By means of this circuit, common-mode HF currents can be evaluated.

The coil-to-ground sinusoidal impedance has been measured connecting the instrument between a coil terminal and the motor frame, being the other coil terminal floating. The results obtained for a set of different coils show a capacitive coupling substantially independent of the excitation frequency. On the contrary, the equivalent series resistance shows two peaks at frequencies corresponding to the parallel resonances. With reference to the test coil, the measured coil-to-ground capacitance C_{tg} was about 82 pF. As a consequence, a three-terminal equivalent circuit can be defined introducing two additional capacitances $C_{tg}/2$ to the equivalent circuit of Fig. 9. These capacitances are connected between each of the two coil terminals and the ground as it is shown in Fig. 12.

In order to fit the model with the experimental results, the previously estimated values of the parallel resistances and parasitic parallel capacitances must be adjusted. At the same time, the model parameters must fit the sinusoidal impedance between the two coil terminals, as discussed in Section III.B. The identification procedure leads to the parameter values reported in Table IV of the Appendix. In Fig. 13, the measured and calculated values of the equivalent series parameters R_s and $|X_s|$ of the sinusoidal impedance between a coil terminal and the ground are shown. Fig. 14 shows the magnitude of this impedance.

It should be noted that the three-terminal equivalent circuit represented in Fig. 12 can be employed to model both the sinusoidal impedance between the two terminals of the coil and that between the coil and the iron core.

When two or more coils are connected in series, such as in a phase of AC stator windings, the series of the single coil models can be used to represent the winding. In this case, to achieve a very accurate HF analysis, the capacitive coupling among the coils should be considered in addition to the magnetic coupling.

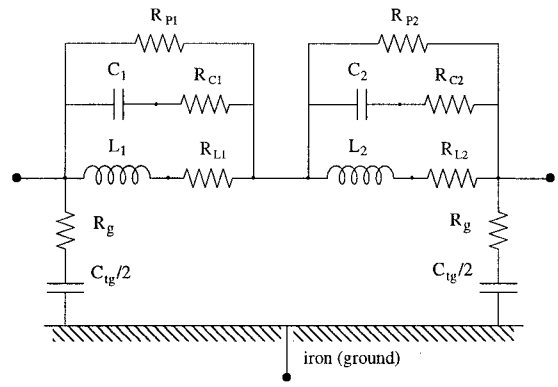

Fig. 12. Three-terminal HF equivalent circuit of the coil

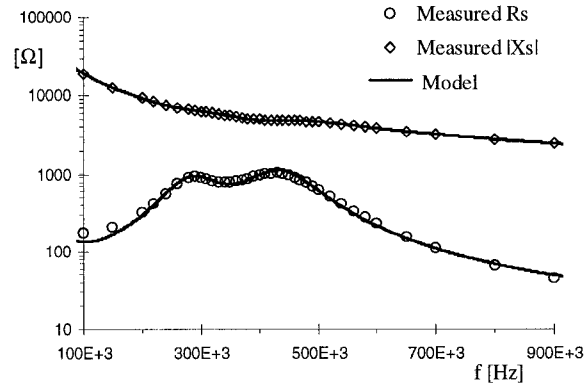

Fig. 13. Measured and calculated R_S and $|X_S|$ between a coil terminal and the ground

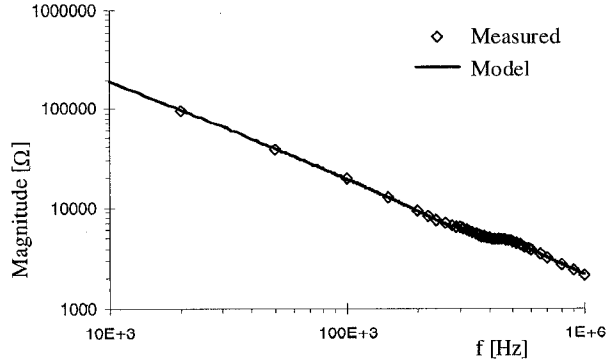

Fig. 14. Measured and calculated impedance between a coil terminal and the ground

IV. CONCLUSIONS

A lumped parameter equivalent circuit for mush wound coils of AC windings has been presented. The proposed model is useful for HF analysis in a wide frequency range. It takes account of turn-to-turn and turn-to-iron stray capacitances and dissipative phenomena due to eddy currents in the coil wires and the laminated iron core. The coil model allows both common- and differential-mode HF current components to be predicted. The equivalent circuit has been fitted with the experimental results obtained by sinusoidal impedance measurements on a test coil. The numerical results have been compared with experimental data showing a good agreement in a wide frequency range.

The model of a multi-coil AC motor winding can be readily obtained by the cascade connection of single coil equivalent circuits. This model can also be used to evaluate the fast-fronted voltage distribution along the winding of an inverter-fed AC motor.

REFERENCES

[1] M.T. Wright, S.J. Yang, K. McLeay, "General Theory of Fast-Fronted Interturn Voltage Distribution in Electrical Machine Windings," *IEE Proc. Part. B*, Vol. 130, No. 4, July 1983, pp. 245-256.

[2] J.L. Guardado, K.J. Cornick, "A Computer Model for Calculating Steep-Fronted Surge Distribution in Machine Windings,"*IEEE Trans*, Vol.EC-4, No.1, March 1989, pp. 95-101.

[3] H. Oraee, P.G. McLaren, "Surge Voltage Distribution in Line-End Coils of induction Motors," *IEEE Trans.*, Vol. PAS-104, No. 7, July 1985, pp. 1843-1848.

[4] R.G. Rhudy, E.L. Owen, D.K. Sharma, "Voltage Distribution Among the Coils and Turns of a Form Wound AC Rotating Machine Exposed to Impulse Voltage," *IEEE Trans.*, Vol. EC-1, No. 2, June 1986, pp. 50-60.

[5] A. Consoli, G. Oriti, A. Testa, A.L. Julian, "Induction Motor Modeling for Common Mode and Differential Mode Emission Evaluation," *Proc. of IAS Conference*, October 1996, Vol. 1, pp. 595-599.

[6] L. Gubbala, A. von Jouanne, P. Enjeti, C. Singh, H. Toliyat, "Voltage Distribution in the Windings of an AC Motor Subjected to High dv/dt PWM Voltages," *Proc. of PESC Conference*, June 1995, pp. 579-585.

[7] E. Zhong, S. Chen, T.A. Lipo, "Improvements in EMI Performance of Inverter-Fed Motor Drives," *Proc. of APEC*, March 1994, pp. 608-614.

[8] C.R. Paul: *Electromagnetic Compatibility*. John Wiley, New York: 1992.

[9] H.A. Haus and J.R. Melcher: *Electromagnetic Fields and Energy*. Prentice Hall, New Jersey: 1989.

[10] F. de Leon and A. Semlyen, "Time Domain Modeling of Eddy Current Effects for Transformer Transients", *IEEE Trans.*, Vol. PD-8, No. 1, January 1993, pp. 271-280.

[11] G. Grandi, A. Massarini, M.K. Kazimierczuk, U. Reggiani, "Capacitances of Single-Layer Air-Core Inductors for High-Frequency Applications," *Proc. of IAS Conference*, October 1996, Vol. 3, pp. 1384-1388.

APPENDIX

Self and mutual partial inductances of a rectangular loop having side lengths a and b and wire radius r_c [7]:

$$L^*_{pa} = \frac{\mu_o}{2\pi} a \left\{ \ln\left[\frac{a}{r_c} + \sqrt{\left(\frac{a}{r_c}\right)^2 + 1} \right] + \frac{r_c}{a} - \sqrt{\left(\frac{r_c}{a}\right)^2 + 1} \right\}$$

$$L^*_{pb} = \frac{\mu_o}{2\pi} b \left\{ \ln\left[\frac{b}{r_c} + \sqrt{\left(\frac{b}{r_c}\right)^2 + 1} \right] + \frac{r_c}{b} - \sqrt{\left(\frac{r_c}{b}\right)^2 + 1} \right\}$$

$$M^*_{pa} = \frac{\mu_o}{2\pi} a \left\{ \ln\left[\frac{a}{b} + \sqrt{\left(\frac{a}{b}\right)^2 + 1} \right] + \frac{b}{a} - \sqrt{\left(\frac{b}{a}\right)^2 + 1} \right\}$$

$$M^*_{pb} = \frac{\mu_o}{2\pi} b \left\{ \ln\left[\frac{b}{a} + \sqrt{\left(\frac{b}{a}\right)^2 + 1} \right] + \frac{a}{b} - \sqrt{\left(\frac{a}{b}\right)^2 + 1} \right\}$$

TABLE I
MAIN COIL AND SLOT DIMENSIONS [mm]

D_h	h	d_a	d_{ir}	D_s	D_c	d_w
82	32.2	10	75	11	9	0.9

TABLE II
MODEL PARAMETERS (AIR-CORE COIL)

L^* [μH]	R^*_L [Ω]	C^* [pF]	R^*_C [Ω]	R^*_p [kΩ]
1030	25	132	8	180

TABLE III
MODEL PARAMETERS (REAL COIL)

L_1, L_2 [μH]	R_{L1}, R_{L2} [Ω]	C1, C2 [pF]	R_{C1}, R_{C2} [Ω]	R_{p1}, R_{p2} [kΩ]
550, 600	120, 140	245, 520	4, 4	5.2, 4.6

TABLE IV
THREE-TERMINAL MODEL PARAMETERS (REAL COIL)

L_1, L_2 [μH]	R_{L1}, R_{L2} [Ω]	C1, C2 [pF]	R_{C1}, R_{C2} [Ω]	R_{p1}, R_{p2} [kΩ]	R_g, C_{gt} [Ω], [pF]
550, 600	120, 140	225, 500	8, 8	6.3, 4.2	8, 82